# Human RF-EMF Exposure Assessment due to Access Point in Incoming 5G Indoor Scenario

Marta Bonato, *Student Member, IEEE*, Laura Dossi, Emma Chiaramello, Serena Fiocchi, Silvia Gallucci, Gabriella Tognola, Paolo Ravazzani, *Member, IEEE* and Marta Parazzini, *Member, IEEE*

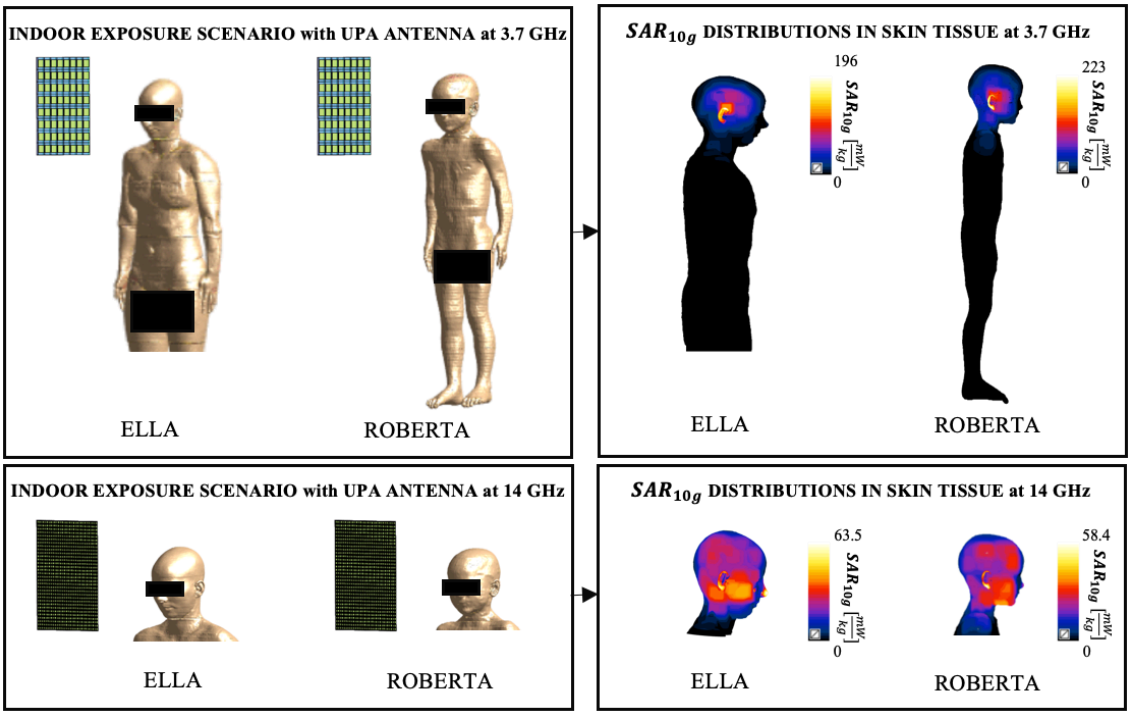


Assessment of RF-EMF exposure levels in incoming 5G indoor scenarios using deterministic computational dosimetry.

**Take-Home Messages**

- Two different indoor uniform planar array (UPA) antennas at 3.7 GHz and at 14 GHz were modelled to simulate the presence of a 5G Access Point (AP) in a room. Two different human models and some different configuration scenarios were considered, where the UPA antennas gain was maximized to obtain the RF-EMF exposure assessment.
- The highest $SAR_{10g}$ levels were obtained in the head area for all the exposure scenarios and the highest $SAR_{10g}$ peak values were measured when the UPA was placed laterally to the human model.
- The work highlighted that the reciprocal position between the antenna and the model head, but also the frequency range and the distance, are factors that could greatly influence the levels of exposure.
- The targeted biological applications are the calculated $SAR_{10g}$ distributions in some specific tissues of the two human models, due to the exposure to a 5G Access Point (AP).
- The study permitted to expand the knowledge about the RF-EMF exposure assessment on a single user, considering the novelties introduced by the incoming 5G networks in indoor scenarios.

# Human RF-EMF Exposure Assessment due to Access Point in Incoming 5G Indoor Scenario

Marta Bonato, *Student Member, IEEE*, Laura Dossi, Emma Chiaramello, Serena Fiocchi, Silvia Gallucci, Gabriella Tognola, Paolo Ravazzani, *Member, IEEE* and Marta Parazzini, *Member, IEEE*

***Abstract*** The study aimed at expanding the knowledge about the assessment of radio-frequency electromagnetic fields (RF-EMF) exposure, considering the novelties introduced by the incoming 5G networks. Specifically, a possible future case of indoor exposure scenario is investigated, where the presence of a 5G access point (AP) in a room is simulated. The AP was modelled by two different indoor uniform planar array (UPA) antennas at 3.7 GHz and at 14 GHz, to evaluate how the beamforming and the higher frequency use could impact the exposure levels. Different scenarios were evaluated, considering the maximum antenna gain, two different human computational models, an adult model and a child one, and by varying the distance and the orientation between the UPA antenna and the two models head. All the simulations were conducted using the Sim4Life platform and in particular the exposure levels were expressed by the specific absorption rate averaged on 10 g of tissue ($SAR_{10g}$), which was analyzed for the skin and for some specific tissues. The work underlined that the highest $SAR_{10g}$ values were obtained in the head area for all scenarios, with the skin $SAR_{10g}$ highest peaks when the UPA is placed laterally to the human model (195.73 mW/kg and 223.29 mW/kg for the adult and child model, respectively, for 100 mW input power). Furthermore, the work permitted to highlight that the $SAR_{10g}$ exposure levels are slightly higher for the child model, compared to the adult one and that the distance between the UPA antenna and the human models could greatly lower the $SAR_{10g}$ levels. At last, it was found that the $SAR_{10g}$ exposure levels obtained with the UPA antenna at 14 GHz were lower than the ones at 3.7 GHz, although further investigations will be necessary.

***Keywords*** **— RF-EMF, indoor exposure, 5G access point, human models, computational dosimetry**

## I. Introduction[1]

THE future will be characterized by the deployment of the 5th generation of mobile networks, which will represent a significant evolution compared to the previous 4th generation (4G) long term evolution (LTE) networks. In particular, the next 5G networks has been designed to satisfy new requirements such as higher data rate increase, low latency and higher number of connected devices and will renew the world where we live in, bringing new services, utilities and benefits to the whole population and to the automotive, health and industry sectors. Indeed, the 5G networks will characterize the idea of future smart homes, cities and societies, for developing the world of Internet of Things devices' connections [1-4]. Initially the 5G networks will be coupled with the existing 4G networks, before the evolution to the fully standalone deployment. Furthermore, to satisfy all these new technology requirements, the 5G networks will be characterized by the use of additional spectrum, in the range between 3 to 100 GHz. In particular, for the Italian country, the first new licensed frequency ranges will be between 3.6–3.8 GHz and 26.5–27.5 GHz [5].

The use of these higher frequencies will imply the possibility to deploy more dense networks characterized by smaller cells at the Base Station (BS) and will result in the development of higher multi-element antenna arrays. These antenna arrays will be implemented not only at the BS in the outdoor environment, benefitting of the massive Multiple Input Multiple Output (MIMO) technology [6, 7], but also much closer to the users in the indoor scenario, where many Access Points (APs) will serve short range areas using dense small cells deployments [8-10]. The use of multi-element antennas will be fundamental also to counterbalance the major problem of very high path loss that signals will experience at new 5G frequencies; in fact, the beamforming capability of antenna arrays will permit to obtain high focalized beams with the benefit of countermeasure the severe path loss with high antenna gain in the desired direction and reduce the network interference and the electromagnetic emission towards other directions [11-13].

Although 5G networks promise to provide benefits for all the population, it is also undeniable that it happens at the expense of drastic changes on the user exposure conditions to the RF-EMF [14, 15]. Therefore, it is clear that the 5G networks deployment is raising questions and worries from the general public and it is thus necessary to conduct promptly an exposure assessment, considering the new antenna technologies and frequencies involved [5, 16].

In literature there are some studies on the exposure levels evaluation of the exposure levels considering the next 5G networks deployment. Some works focused on the exposure assessment considering the introduction of the new 5G frequency ranges [17-19], evaluating the exposure levels in simplified models; others on specific devices that will

All authors are with the Institute of Electronics, Computer and Telecommunication Engineering (IEIIT), CNR, Milano, Italy (e-mail: marta.bonato@ieiit.cnr.it,laura.dossi@ieiit.cnr.it,emma.chiaramello@ieiit.cnr.it,serena.fiocchi@ieiit.cnr.it,silvia.gallucci@ieiit.cnr.it,gabriella.tognola@ieiit.cnr.it,paolo.ravazzani@ieiit.cnr.it, marta.parazzini@ieiit.cnr.it).

M.B. and S.G. are also with the Department of Electronics, Information and Bioengineering (DEIB), Politecnico di Milano, Italy.

involve the use of the new 5G technology for the uplink scenario [20-22]. Furthermore, considering the downlink scenario, the literature studies focused on the exposure assessment due to the deployment of massive MIMO BS in outdoor scenarios [23-25], whereas others focused on the indoor environments, considering that the 5G innovations will be deployed also for indoor BS (Access Point AP), closer to the users [26-28]. Among them, Shikhantsov et al. [27, 28] evaluated the exposure levels in a human model considering two different downlink indoor scenarios. The first work [27] assessed the exposure caused by an indoor massive MIMO BS at 3.5 GHz in an industrial environment and the second one [28] was focused on a prospective 5G wireless networking technology, in which humans are exposed by several interfering sources at 3.5 GHz.

Therefore, the present paper fits into this contest with the aim to expand the knowledge on the exposure levels considering the novelties of the incoming 5G network, focusing on a specific case of indoor scenario. In particular, we simulated an indoor scenario with an AP with some 5G networks, i.e. a dense microcell deployment, new frequency ranges and beamforming capability. The AP was in fact modelled by two different models of uniform planar array (UPA) antennas. The first model of UPA antenna was characterized by 64 patch elements at 3.7 GHz, in the range of the first licensed frequencies in Italy, whereas the second model involved an UPA antenna with 1024 elements at 14 GHz, to evaluate how an increase in the operation frequency could impact on the exposure levels. The downlink exposure levels were assessed considering the case where the UPA antenna gain was maximized. To evaluate how the user's age could impact on the level of exposure, two different human models were used, one of an adult and one of a child and it was decided to direct the primary beam of the UPA antenna towards the head area of both models. Furthermore, we repeated some simulations for different configurations and distances between the UPA antenna and the head models to verify the impact of these factors on the levels of exposure. For all the simulated conditions, the human exposure levels were assessed and compared by evaluating the specific absorption rate ($SAR$), a quantity indicated also in the ICNIRP guidelines [29]. More in specific, the distributions of $SAR$ mediated on 10 g were evaluated for all the domain of interest and for some specific tissues.

## II. Materials and Methods

### A. Antenna Design

For the antenna design we started from our previous work [30] and in particular, as shown in the upper part of Fig.1, the access point located in the room was modelled firstly by an indoor UPA antenna with 64 elements. More specifically, each element of the UPA antenna was characterized by a simple patch antenna composed by three layers. The dielectric properties of the three layers were chosen according to data in literature [28]. In specific, the ground and patch layers were modelled as PEC materials, whereas the substrate element was modelled by a dielectric material (dielectric properties: $\varepsilon_r = 2.25$ and $\sigma = 0.0005\ S/m$).

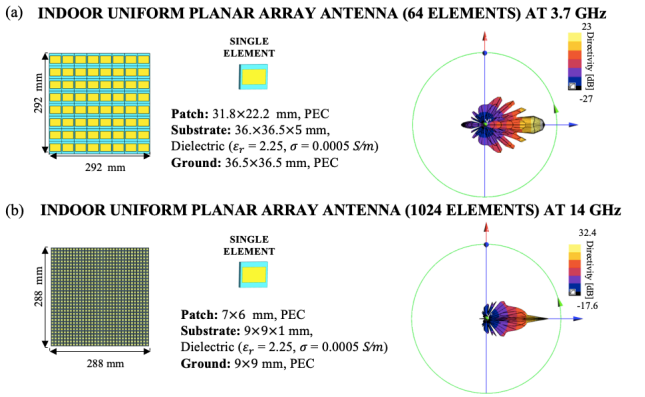


Fig. 1. (a) In the left part, the design and the dimensions of the indoor UPA antenna with 64 elements at 3.7 GHz and the single patch antenna details. In the right part, the directivity diagram in the air. (b) In the left part, the design and the dimensions of the indoor UPA antenna with 1024 elements at 14 GHz and the single patch antenna details. In the right part, the directivity diagram in the air.

The dimensions of the single patch antenna are reported in Fig.1, resulting in a total dimension of the UPA antenna of around 29x29x0.5 cm. The choice of the dimensions and the antenna model have been carried out in order to have a resonance of the array antenna at 3.7 GHz. At last, the UPA antenna was driven by an input power port of 100 mW in total, in line with the specifications of 3rd Generation Partnership Project [31], the phase shift between the different array elements was set to zero and all the elements of the antenna were excited simultaneously with a gaussian signal.

In this way, as it is illustrated in upper part of Fig.1, the main lobe of the array antenna is in the boresight direction, i.e. perpendicular to the plane of the antenna, so providing the maximum gain. As it can be seen from the above part of Fig.1, to evaluate the impact of the operation frequency on the exposure levels, we also modelled an access point at 14 GHz. In this case, the 5G indoor access point was modelled by an indoor UPA antenna with 1024 elements at 14 GHz. The total number of the patch antennas and their dimension were chosen in order to obtain an array antenna with a resonance at 14 GHz but with the total dimensions comparable with the one at 3.7 GHz, i.e. 28.8x28.8x0.1 cm. The phase shift between the elements and the total input power of the array antenna remained the same as the array antenna at 3.7 GHz. As shown in Fig.1, decreasing the wavelength, the directivity of the antenna increases, showing a sharper perpendicular lobe respect to the case at 3.7 GHz.

### B. Exposure Simulations

All the simulations were implemented with the finite-difference time-domain (FDTD) solver of the simulation platform SIM4life (ZMT Zurich Med Tech AG, Zurich, Switzerland, www.zurichmedtech.com). Ella and Roberta human models from the Virtual Population [32] were used, as it is shown in Fig.2. Ella represents an average female adult (age = 26 years old, height =1.63 $m$, mass = 57.3 $kg$, BMI= 21.6 $kg/m$), whereas Roberta characterizes a child (age = 5 years old, height =1.1 $m$, mass = 17.6 $kg$, BMI= 14.8 $kg/m$).

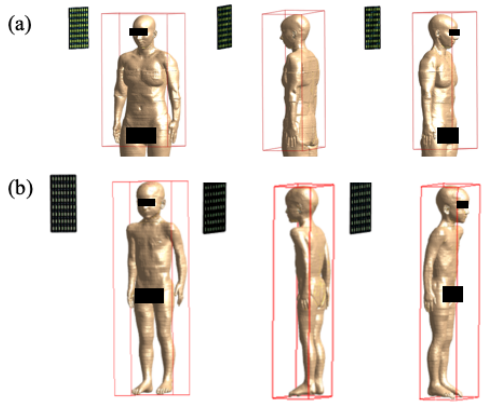


Fig. 2. Example of the three different examined configurations for the indoor 64 elements UPA antenna at 3.7 GHz. (a) For Ella model (the red box indicates the domain of interest in the model). (b) For Roberta model (the red box indicates the domain of interest in the model).

The tissues dielectric properties of Ella and Roberta were chosen according to literature [33, 34], considering the chosen frequencies of 3.7 GHz and of 14 GHz.

For the UPA antenna at 3.7 GHz, the computational domain included the antenna and the human model, but this last was limited to the head and torso area in the case of Ella (as evidenced by a red box in Fig. 2a), whereas for Roberta the full body was included. The computational domain was discretized with a nonuniform grid with a maximum step of 0.9 mm for the human bodies, to correctly discretize all the tissues, resulting in a maximum total number of about $180 \times 10^6$ discretization cells. The computational domain was truncated by assuming a perfectly matched layer (PML) absorbing condition at the domain boundaries.

In the case of 14 GHz UPA antenna, the computational domain was limited to the head area for both models, due to computational costs (the total number of cells were in fact of about $1 \times 10^9$). The domain was discretized with a nonuniform grid with a maximum step of 0.4 mm for both the human bodies, applying the same PML absorbing condition at the domain boundaries.

### C. *Exposure Scenarios*

The configurations for the 5G exposure scenario at 3.7 GHz were chosen in order to have the main lobe of the UPA antenna pointing towards the models' head for different reciprocal positions of the head and the antenna, to assess which configuration caused the highest exposure levels. For this reason, for both models, three different configurations were examined, as it is shown in Fig. 2. In the first configuration, the antenna is placed laterally to the head model, in the second one is placed in front of the head model and in the third one posteriorly to the head model. The distance between the subject and the UPA antenna remained the same for all three configurations and for both models and was equal to 50 cm from the central head point of the model.

To evaluate how the distance between the source and the human model could impact on the exposure levels in 5G indoor exposure scenario, for the lateral configuration the simulations were repeated for a distance between the antenna and the central head point of both the models equal to 1 m, fixed the other parameters (input power and phase shift).

Finally, to evaluate the impact of the frequency, the exposure levels were estimated considering an access point equipped with a modelled 1024-elements array antenna at 14 GHz, for both human models in the lateral configuration at a distance of 50 cm from the antenna.

### D. *Exposure Assessment*

To express and to compare the head exposure levels, in all the scenarios and for both human models, we decided to evaluate the distributions of the Specific Absorption Rate averaged on 10 g of tissue (indicated from now on as $SAR_{10g}$), with particular interest to the skin, the eyes tissues and brain tissues. More specifically, for the skin tissues, the $SAR_{10g}$ distributions were examined considering either the head and torso body regions taken together or limiting the body region to the head area only, supposed to be the body area primarily exposed to the beam of the UPA antenna. As for the eyes tissues, the $SAR_{10g}$ distributions were assessed considering the cornea, sclera, lens and humor vitreous for both models. Finally, the $SAR_{10g}$ distributions were assessed considering the whole brain (which included for Ella's brain grey matter, brain white matter, hippocampus, hypophysis, hypothalamus, medulla oblongata, midbrain, pineal body, pons, thalamus, commissure anterior and posterior, and for Roberta's the same tissues except for the commissure anterior and posterior), the brain grey matter alone and the cerebellum. The $SAR_{10g}$ distributions in the skin, eyes and brain tissues were displayed calculating for each tissue the boxplot. Furthermore, to better quantify the $SAR_{10g}$ distributions, the following quantities were calculated for each tissue: the maximum, median, mean values, quartile coefficient of dispersion ($QCD = (Q_3 - Q_1)/(Q_3 + Q_1)$, where $Q_1$ and $Q_3$ are, respectively, the first and third quartiles of the distribution) and at last the skewness and the kurtosis indexes.

## III. RESULTS

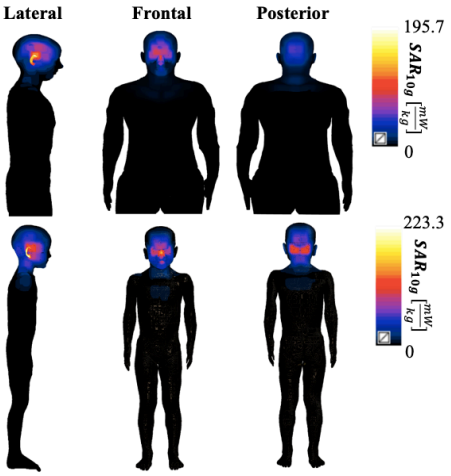


Fig. 3. Distribution of the $SAR_{10g}$ in the skin domain induced by the indoor 64 elements UPA antenna at 3.7 GHz at a distance of 50 cm from the head model for the three different configurations, in the upper panels for Ella and in the lower panels for Roberta.

In Fig. 3 are shown the distributions of $SAR_{10g}$ on the skin at 3.7 GHz for 100 mW input power, with a distance of 50 cm between the antenna and the head model in the three configurations, for Ella in the upper part and for Roberta in the lower part. It can be easily noticed that the distributions have a similar trend between the two models. The highest $SAR_{10g}$ values were obtained in the head area, whereas the torso (and also the limbs for Roberta) showed almost null values for both models and in all the exposure scenarios. Specifically, the highest values were individuated in the head region closer to the UPA antenna, namely in the ears area for the lateral configuration, in the nose and eyes area for the frontal one and in the occipital region of the head closed to the cerebellum for the posterior one.

For better characterizing the exposure levels, Fig. 4 reports the boxplot of the $SAR_{10g}$ distributions for each examined tissue in both models, considering the three different configurations at 3.7 GHz, 64-elements antenna and a distance of 50 cm from the antenna. Furthermore, to better quantify the same $SAR_{10g}$ distributions, Tab. I reports maximum, median, mean values and $QCD$, skewness and kurtosis indexes. As it can be seen from both the boxplots in Fig. 4 and the values in Tab. I, among the different tissues the highest $SAR_{10g}$ values were obtained in the skin tissue, more precisely in the head region (the peak values of the head skin were in fact the same of the one found in the head and torso skin region). For Ella, the peak values for skin are 195.73 mW/kg, 100.29 mW/kg and 50.44 mW/kg, respectively for lateral, frontal and posterior configurations. It means that the lowest skin peak value, obtained in the posterior configuration, is about ¼ of the highest value obtained in the lateral one. The same trend was found for Roberta, although the peak values in the three exposure configurations were slightly higher compared to the ones found in Ella (223.29 mW/kg, 159.49 mW/kg and 112.64 mW/kg respectively for the lateral, frontal and posterior configurations), and the decrease from the highest to the lowest peak values was of about ½. Furthermore, it was found that the median and mean values for the skin of the head region only (mean values of 11.21 mW/kg, 8.11 mW/kg, 8 mW/kg for Ella in the three configurations) are higher compared to the values obtained in the skin tissue that comprises both the head and the torso (1.81 mW/kg, 1.36 mW/kg, 1.36 mW/kg for Ella). Comparing the boxplot distributions of only head skin and of the head and torso region skin, reinforced what we expected that, because of the head position closer to the antenna rather than the torso, for both models the levels evaluated in the head skin only were higher than the levels simulated for the torso and were consequently responsible of the peak values evaluated for the skin in the whole domain. This is less obvious for the whole brain tissues compared to brain grey matter alone but the trend is similar. In fact, also in this case, the maximum values obtained for the whole brain coincided with the maximum values for the brain grey matter, and the median and mean values for the brain grey matter were greater than the values

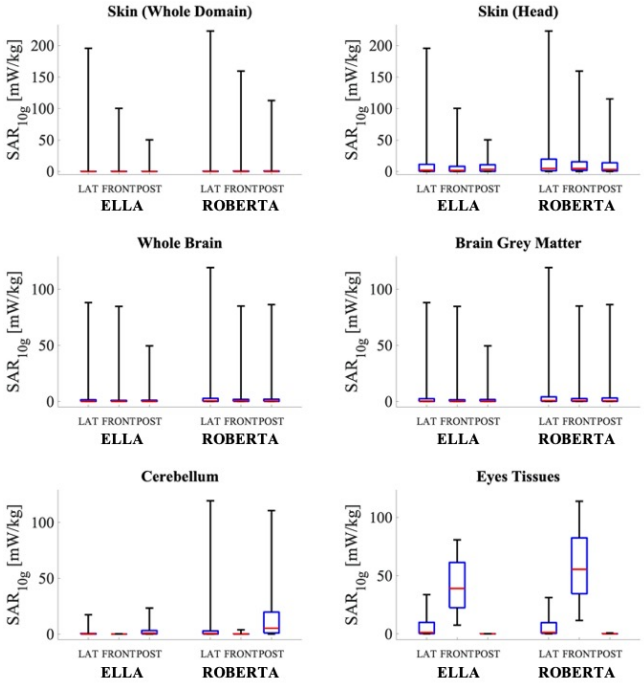


Fig.4. Boxplots of the $SAR_{10g}$ distributions in the tissues of interest for both the Ella and Roberta models, considering the indoor 64 elements UPA antenna at 3.7 GHz at a distance of 50 cm from the head model for the three different configurations. The lower and upper bounds of the box represent the first and the third quartiles, the red line is the median value, and the whiskers are the minimum and maximum values of the distribution.

for the whole brain. Interestingly, the lateral and frontal configurations gave quite similar peak values in the brain grey matter for Ella (88.1 mW/kg and 84.73 mW/kg, with 49.47 mW/kg for the posterior exposure), whereas for Roberta's model similar values were found for the frontal and posterior configurations (85.06 mW/kg and 86.33 mW/kg, with 119.33 mW/kg in the lateral one). The values obtained for the cerebellum and the eyes tissues highlighted that the reciprocal position between the UPA antenna and the model head could greatly affect their levels of exposure. For example, the peak values for Ella in the eyes tissues vary from 80.76 mW/kg in the frontal configuration, where the UPA antenna is definitely closer to these tissues, to 0.12 mW/kg and 33 mW/kg in posterior and lateral ones, with a percentage reduction of respectively 99.9% and 58%. For Roberta, the percentage reductions were around 99.4% and 72.6%, respectively. Furthermore, as it can be seen from Tab. I, the highest median and mean values for the cerebellum were obtained for both the models in the posterior configuration, where the UPA antenna is closer to this tissue, with a particular increase especially in Roberta, which also presented the maximum exposure value for the lateral configuration, as it can be noticed from the boxplot in Fig. 3.

In general, for both models the mean and median values deviated significantly from the maximum values and had much lower values in the whole tissues under investigation. Furthermore, the $QCD$, skewness and kurtosis indexes revealed high values in almost all tissues and configurations, which indicates the data show high degree of variation and strongly deviate from being normally distributed.

TABLE I
ESTIMATED QUANTITIES FROM THE $SAR_{10g}$ DISTRIBUTIONS FOR THE ELLA AND ROBERTA MODELS AT 3.7 GHZ

| | | ELLA | | | ROBERTA | | |
|---|---|---|---|---|---|---|---|
| **Tissue** | **Parameter** | **LAT** | **FRONT** | **POST** | **LAT** | **FRONT** | **POST** |
| Skin *(Whole Domain)* | Maximum (mW/kg) | 195.73 | 100.29 | 50.44 | 223.29 | 159.49 | 112.64 |
| | Median (mW/kg) | <0.01 | 0.01 | <0.01 | 0.02 | 0.04 | 0.05 |
| | Mean (mW/kg) | 1.81 | 1.36 | 1.36 | 2.40 | 2.04 | 2.02 |
| | QCD | ~1 | ~1 | ~1 | ~1 | ~1 | ~1 |
| | Skewness | 8.91 | 8.39 | 6.03 | 8.68 | 7.99 | 8.22 |
| | Kurtosis | 101.35 | 81.10 | 43.64 | 102.45 | 84.62 | 84.90 |
| Skin *(Head)* | Maximum (mW/kg) | 195.73 | 100.29 | 50.44 | 223.29 | 159.49 | 112.64 |
| | Median (mW/kg) | 1.98 | 1.51 | 3.17 | 4.55 | 4.56 | 3.12 |
| | Mean (mW/kg) | 11.21 | 8.11 | 8.00 | 16.98 | 13.94 | 13.22 |
| | QCD | 0.96 | 0.96 | 0.96 | 0.89 | 0.80 | 0.89 |
| | Skewness | 3.21 | 2.86 | 1.87 | 2.79 | 2.45 | 2.50 |
| | Kurtosis | 15.12 | 10.95 | 5.96 | 12.46 | 9.78 | 9.35 |
| Whole Brain | Maximum (mW/kg) | 88.10 | 84.73 | 49.47 | 119.33 | 85.03 | 86.33 |
| | Median (mW/kg) | 0.19 | 0.14 | 0.14 | 0.50 | 0.40 | 0.37 |
| | Mean (mW/kg) | 2.27 | 1.38 | 1.62 | 4.12 | 2.45 | 3.25 |
| | QCD | 0.98 | 0.97 | 0.98 | 0.95 | 0.93 | 0.96 |
| | Skewness | 4.44 | 5.72 | 4.27 | 4.41 | 5.11 | 4.27 |
| | Kurtosis | 27.80 | 52.37 | 25.23 | 29.15 | 35.92 | 23.93 |
| Brain Grey Matter | Maximum (mW/kg) | 88.10 | 84.73 | 49.47 | 119.33 | 85.03 | 86.33 |
| | Median (mW/kg) | 0.28 | 0.26 | 0.25 | 0.71 | 0.62 | 0.58 |
| | Mean (mW/kg) | 3.03 | 1.89 | 1.99 | 5.33 | 3.18 | 4.06 |
| | QCD | 0.98 | 0.96 | 0.97 | 0.95 | 0.91 | 0.95 |
| | Skewness | 3.74 | 4.84 | 3.87 | 3.78 | 4.40 | 3.74 |
| | Kurtosis | 19.86 | 37.75 | 21.36 | 21.73 | 26.67 | 18.80 |
| Cerebellum | Maximum (mW/kg) | 17.35 | 0.20 | 23.25 | 119.33 | 3.82 | 110.63 |
| | Median (mW/kg) | 0.05 | <0.01 | 0.82 | 0.52 | 0.03 | 5.27 |
| | Mean (mW/kg) | 0.77 | 0.01 | 2.32 | 4.21 | 0.09 | 13.72 |
| | QCD | 0.97 | 0.96 | 0.90 | 0.94 | 0.94 | 0.91 |
| | Skewness | 3.53 | 3.78 | 2.00 | 2.91 | 3.14 | 1.85 |
| | Kurtosis | 17.71 | 20.73 | 7.03 | 11.79 | 25.98 | 6.26 |
| Eyes Tissues | Maximum (mW/kg) | 33.68 | 80.76 | 0.12 | 31.17 | 113.72 | 0.74 |
| | Median (mW/kg) | 1.12 | 38.93 | 0.03 | 1.17 | 55.39 | 0.06 |
| | Mean (mW/kg) | 5.81 | 40.66 | 0.03 | 5.66 | 57.21 | 0.09 |
| | QCD | 0.95 | 0.47 | 0.57 | 0.92 | 0.41 | 0.55 |
| | Skewness | 1.29 | 0.01 | 1.04 | 1.08 | <0.01 | 2.52 |
| | Kurtosis | 3.78 | 1.54 | 3.38 | 3.09 | 1.60 | 11.41 |

In particular, these parameters permitted to highlight that for the widest examined tissues (e.g. whole domain skin, whole brain and brain grey matter), almost the totality of the values concentrated in a range from zero to one hundredth of the maximum. The $SAR_{10g}$ distributions in these tissues were in fact strongly skewed to the values near zero and the percentage of values higher than the mean was in fact around only 10-11% for the skin, around 20% for whole brain and around 22-23% for the brain grey matter, depending on the exposure configurations. Considering the head only skin domain and the tissues with a smaller extension (e.g. cerebellum and in particular eyes tissue), the distributions become smoother and less skewed, strongly depending on the configuration under examination, as it can be noticed from the skewness and the kurtosis indexes in Tab. I and the boxplot in Fig.4. For example, the percentage of values higher than the mean is equal to 30% for the cerebellum in the posterior configuration and increases until 47% in the eyes tissues in the frontal configuration, where the $SAR_{10g}$ distributions are almost normal for the two models, although even in those cases the percentage of values close to the maximum remained very limited.

The above simulations, with same antenna array, same frequency, same input power and same two models, have been repeated in the lateral configuration, moving away the UPA antenna at a distance of 1 m from the central head point. Compared to the results obtained for a distance of 50 cm, the peak values of the $SAR_{10g}$ skin distributions decreased from 195.75 mW/kg and 223.29 mW/kg to 0.14 mW/kg and 0.07 mW/kg for Ella and Roberta, respectively. This drastic reduction of around almost the 99.9% on the exposure levels was consistent across all the tissues examined.

Finally, Tab. II reports the results simulated with the UPA antenna with 1024 elements at 14 GHz with 100 mW input power, for both models in the lateral configuration (the figures of $SAR_{10g}$ distributions and boxplots could be found in the supplementary material section). The $SAR_{10g}$ maximum values are again in the head skin tissue, for both models ($SAR_{10g}$ peak values equal to 63.46 mW/kg and 58.40 mW/kg and maximum absorbed power density averaging on a square area of 4 $cm^2$ of skin tissue equal to 0.98 $W/m^2$ and 1.8 $W/m^2$ for Ella and Roberta respectively). The comparison of these results with the results obtained at the frequency of 3.7 GHz highlighted how the use of a higher frequency drastically lowered the maximum $SAR_{10g}$ levels in the skin tissue of about the 67.6% in Ella and about the 73.8% in Roberta. From the values shown in Tab. II, it could be noticed that also in this case Roberta's mean and median values are slightly higher than those of Ella, with the only exception of the eyes tissues. Furthermore, the QCD, skewness and kurtosis values reported in Tab. II confirmed that also at 14 GHz the distributions are highly left skewed, with the only exception of the head skin tissue, which presented a smoother distribution.

TABLE II
ESTIMATED QUANTITIES FROM THE $SAR_{10g}$ DISTRIBUTIONS FOR THE ELLA AND ROBERTA MODELS AT 14 GHZ

| | | ELLA | ROBERTA |
|---|---|---|---|
| **Tissue** | **Parameter** | **LAT** | **LAT** |
| Skin *(Head)* | Maximum (mW/kg) | 63.46 | 58.40 |
| | Median (mW/kg) | 1.87 | 6.54 |
| | Mean (mW/kg) | 7.75 | 10.53 |
| | QCD | 0.99 | 0.93 |
| | Skewness | 1.43 | 0.93 |
| | Kurtosis | 4.02 | 2.92 |
| Whole Brain | Maximum (mW/kg) | 26.32 | 29.98 |
| | Median (mW/kg) | <0.01 | <0.01 |
| | Mean (mW/kg) | 0.17 | 1.15 |
| | QCD | 0.99 | 0.97 |
| | Skewness | 9.56 | 4.78 |
| | Kurtosis | 126.13 | 26.97 |
| Brain Grey Matter | Maximum (mW/kg) | 26.32 | 29.98 |
| | Median (mW/kg) | <0.01 | <0.01 |
| | Mean (mW/kg) | 0.27 | 1.66 |
| | QCD | ~1 | ~1 |
| | Skewness | 7.54 | 3.90 |
| | Kurtosis | 76.85 | 18.30 |
| Cerebellum | Maximum (mW/kg) | 10.92 | 20.67 |
| | Median (mW/kg) | <0.01 | <0.01 |
| | Mean (mW/kg) | 0.07 | 0.45 |
| | QCD | ~1 | ~1 |
| | Skewness | 11.85 | 5.78 |
| | Kurtosis | 168.43 | 40.08 |
| Eyes Tissues | Maximum (mW/kg) | 26.52 | 20.33 |
| | Median (mW/kg) | 0.30 | 0.25 |
| | Mean (mW/kg) | 4.71 | 2.08 |
| | QCD | 0.99 | 0.97 |
| | Skewness | 1.64 | 2.15 |
| | Kurtosis | 4.19 | 6.57 |

## IV. DISCUSSION

This paper focused on the evaluation of human RF exposure assessment in a possible future case of 5G indoor scenario. The novelty of the paper consists in considering antenna arrays and new higher frequencies that will be introduced by 5G networks. Two different UPA antenna were in fact modelled simulating an indoor 5G AP at 3.7 GHz and at 14 GHz. Two different human models, different reciprocal positions and distances between the antennas and the models were considered, to better characterize the exposure assessment. The analysis was mainly focused on the $SAR_{10g}$ distributions in some specific tissues of interest, that are the skin, the brain tissues, the cerebellum and the eyes tissues. Our simulations highlighted that for the examined configurations the highest $SAR_{10g}$ values were obtained in the head area rather than the torso and limbs area. This result is in line with the decision of directing the main lobe of the boresight antenna toward the models' head, thus making models' head the closest area to the antenna. Furthermore, it was noticed that the most exposed head region is greatly influenced by the reciprocal position between the head and the UPA antenna. The analysis of the $SAR_{10g}$ distributions of the different tissues showed that the highest values occur with a very small percentage, especially considering the largest tissues examined (e.g. skin and whole brain), whereas for the smallest tissues (e.g. eyes, ears, cerebellum) the values distributions showed a smoother trend. In the considered scenarios all the values were well below the exposure limits indicated by the ICNIRP guidelines of 2 W/kg for the local head and torso $SAR$ [29].

Since in the present paper a specific indoor case of exposure scenario was analysed, it is not easy to find in literature previous studies with the same characteristics to make a fair comparison. It remains however interesting to discuss, at least from a qualitative point of view, similarities and differences with other studies which investigated on 5G frequencies or indoor scenario exposure levels. For example, we found that the configuration with the highest $SAR_{10g}$ values was the lateral one, where the UPA antenna at 3.7 GHz is placed on the side respect to the model's head, and this conclusion is in line with the analysis of Shikhantsov et al. [27], where, although the distance between the antenna and the human model was much greater than our analysed cases, the highest exposure values were obtained in the lateral exposure of the head. Additionally, also in the work of Uusitupa et al. [35], where a single-plane wave exposure was considered, the highest exposure values were almost always found in the side-exposure cases. It was in fact underlined that in the GHz region, the typical peak $SAR$ locations were in the fingers, toes, nose, ears, chin, penis and testicles regions, because the field could effectively enter inside these body parts that had relatively small dimensions.

Furthermore, the use of two models with different ages highlighted that the child was characterized by slightly higher exposure $SAR_{10g}$ values respect to the adult, in almost all the examined configurations. The same trend was found in the work of Uusitupa et al. [35], where the exposure levels were assessed considering various human models of different ages and the boy model presented actually the highest values of $SAR$ respect to the adult models. The distance increase between the antenna and the model head resulted, as expected, in lower exposure level. Although the results remained quite intuitive, they permitted to highlight the fact that the distance between the user and the indoor AP was the factor, among the analyzed ones, with the strongest impact on the $SAR_{10g}$ distributions. At last, we showed that increasing the frequency to 14 GHz with a 1024-elements UPA antenna lead to lower the $SAR_{10g}$ values, for both human models, when the antenna was placed lateral to the head, although further specific investigations into absorbed power density levels will be needed in the upcoming studies.

## V. CONCLUSIONS

In conclusion, the aim of the work to further expand the knowledge on the exposure assessment in 5G indoor scenario was achieved. The $SAR_{10g}$ exposure levels were simulated for UPA antennas at 3.7 GHz and 14 GHz, two human models, different reciprocal positions between the antenna and the model head and different distances. In the future, traditional computational methods will be combined with stochastic and machine learning techniques, to extend the exposure assessment for a multitude of exposure scenarios, not limiting the analysis to few worst-cases but facing off with the heterogeneity introduced by 5G networks [36-38].

## APPENDIX

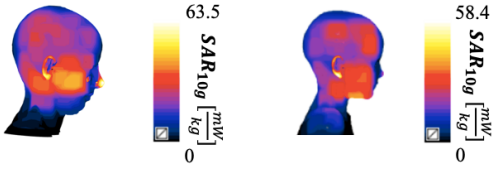


Fig. 5. Distribution of the $SAR_{10g}$ in the skin domain induced by the indoor 1024 elements UPA antenna at 14 GHz with a distance of 50 cm between the antenna and the head model for the lateral configuration, in the left panel for Ella and in the right panel for Roberta.

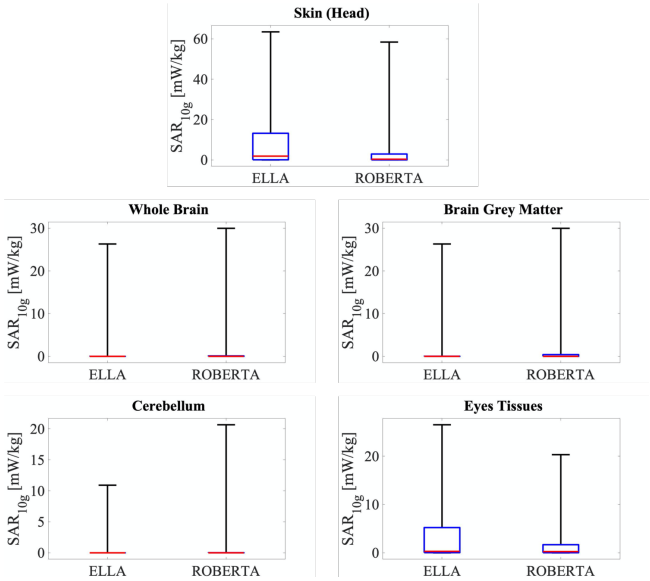


Fig.6. Boxplots of the $SAR_{10g}$ distributions in the tissues of interest for both the Ella and Roberta models, considering the indoor 1024-elements UPA antenna at 14 GHz at a distance of 50 cm from the head model for the lateral configuration. The lower and upper bounds of the box represent the first and the third quartiles, the red line is the median value, and the whiskers are the minimum and maximum values of the distribution.

## ACKNOWLEDGMENT

The authors wish to thank Schmid and Partner Engineering AG (www.speag.com) for having provided the simulation software SIM4Life.

## REFERENCES

[1] J.G. Andrews, S. Buzzi, W. Choi, S.V. Hanly, A. Lozano, A.C. Soong, J.C. Zhang, "What will 5G be?," *IEEE Journal on selected areas in communications,* 2014 Jun 3;32(6):1065-82.

[2] W.H. Chin, Z. Fan, R. Haines, "Emerging technologies and research challenges for 5G wireless networks," *IEEE Wireless Communications*. 2014 May 12;21(2):106-12.

[3] S. Hong, J. Brand, J.I. Choi, M. Jain, J. Mehlman, S. Katti, P. Levis, "Applications of self-interference cancellation in 5G and beyond," *IEEE Communications Magazine*, 2014, Feb 12;52(2):114-21.

[4] F. Boccardi, R.W. Heath, A. Lozano, T.L. Marzetta, P. Popovski, "Five disruptive technology directions for 5G," *IEEE Communications Magazine*. 2014 Feb 12;52(2):74-80.

[5] *Recommendations, ITU-T. K-Series,* "5G technology and human exposure to RF EMF," 2017.

[6] E. G. Larsson, O. Edfors, F. Tufvesson, T.L. Marzetta, "Massive MIMO for next generation wireless systems," *IEEE communications magazine*, 2014 Feb 12;52(2):186-95.

[7] B. Ai, K. Guan, R. He, J. Li, G. Li, D. He, Z. Zhong K.M.S. and Huq, "On indoor millimeter wave massive MIMO channels: Measurement and simulation," *IEEE journal on selected areas in communications*, 35(7), 2017, pp.1678-1690.

[8] S. Deng, M.K. Samimi, T.S. Rappaport, "28 GHz and 73 GHz millimeter-wave indoor propagation measurements and path loss models," *IEEE International Conference on Communication Workshop (ICCW)*, 2015 Jun 8 (pp. 1244-1250).

[9] D. Muirhead, M.A. Imran, K. Arshad, "Insights and approaches for low-complexity 5G small-cell base-station design for indoor dense networks," *IEEE access,* 2015 Aug 27;3:1562-72.

[10] M. Lei, J. Zhang, T. Lei, D. Du, "28-GHz indoor channel measurements and analysis of propagation characteristics," *IEEE 25th Annual International Symposium on Personal, Indoor, and Mobile Radio Communication (PIMRC)*, 2014 Sep 2 (pp. 208-212). IEEE.

[11] S.M. Razavizadeh, M. Ahn, I. Lee, "Three-dimensional beamforming: A new enabling technology for 5G wireless networks," *IEEE Signal Processing Magazine*, 2014 Oct 14;31(6):94-101.

[12] J. Jang, M. Chung, S.C. Hwang, Y.G. Lim, H.J. Yoon, T. Oh, B.W. Min, Y. Lee, K.S. Kim, C.B. Chae, D.K. Kim, "Smart small cell with hybrid beamforming for 5G: Theoretical feasibility and prototype results," *IEEE Wireless Communications,* 2016 Nov 15;23(6):124-31.

[13] S. Han, I. Chih-Lin, Z. Xu, C. Rowell, "Large-scale antenna systems with hybrid analog and digital beamforming for millimeter wave 5G," *IEEE Communications Magazine,* 2015 Jan 16;53(1):186-94.

[14] E. Chiaramello, M. Bonato, S. Fiocchi, G. Tognola, M. Parazzini, P. Ravazzani, J. Wiart, "Radio frequency electromagnetic fields exposure assessment in indoor environments: A Review," *International journal of environmental research and public health*, 2019 Jan;16(6):955.

[15] Y. Huang, J. Wiart, "Simplified assessment method for population RF exposure induced by a 4G network," *IEEE Journal of Electromagnetics, RF and Microwaves in Medicine and Biology,* 2017 Sep 18;1(1):34-40.

[16] C.L. Russell, "5 G wireless telecommunications expansion: Public health and environmental implications," *Environmental research*, 2018 Aug 1;165:484-95.

[17] R. Morimoto, I. Laakso, V. De Santis, A. Hirata, "Relationship between peak spatial-averaged specific absorption rate and peak temperature elevation in human head in frequency range of 1–30 GHz," *Physics in Medicine & Biology*, 2016 Jul 1;61(14):5406.

[18] R. Morimoto, A. Hirata, I. Laakso, M.C. Ziskin, K.R. Foster, "Time constants for temperature elevation in human models exposed to dipole antennas and beams in the frequency range from 1 to 30 GHz," *Physics in Medicine & Biology*, 2017 Feb 6;62(5):1676.

[19] E. Neufeld, E. Carrasco, M. Murbach, Q. Balzano, A. Christ, N. Kuster, "Theoretical and numerical assessment of maximally allowable power-density averaging area for conservative electromagnetic exposure assessment above 6 GHz," *Bioelectromagnetics*, 2018 Dec;39(8):617-30.

[20] B. Thors, D. Colombi, Z. Ying, T. Bolin, C. Törnevik. "Exposure to RF EMF from array antennas in 5G mobile communication equipment," *IEEE Access,* 2016 Aug 17;4:7469-78.

[21] D. Colombi, B. Thors, C. Törnevik, Q. Balzano, "RF energy absorption by biological tissues in close proximity to millimeter-wave 5G wireless equipment," *IEEE Access*, 2018 Jan 5;6:4974-81.

[22] A.R. Guraliuc, M. Zhadobov, R. Sauleau, L. Marnat, L. Dussopt, "Near-field user exposure in forthcoming 5G scenarios in the 60 GHz band," *IEEE Transactions on Antennas and Propagation*, 2017 Nov 3;65(12):6606-15.

[23] P. Baracca, A.Weber, T. Wild, C. Grangeat, "A statistical approach for RF exposure compliance boundary assessment in massive MIMO systems," *WSA 2018; 22nd International ITG Workshop on Smart Antennas,* 2018 Mar 14 (pp. 1-6). VDE.

[24] B. Thors, A. Furuskär, D. Colombi, C. Törnevik. "Time-averaged realistic maximum power levels for the assessment of radio frequency exposure for 5G radio base stations using massive MIMO," *IEEE Access,* 2017 Sep 18;5:19711-9.

[25] I. Nasim, S. Kim. "Mitigation of human EMF exposure in downlink of 5G," *Annals of Telecommunications*, 2019 Feb 1;74(1-2):45-52.

[26] T. Wigren, D. Colombi, B. Thors, J.E. Berg, "Implication of RF EMF exposure limitations on 5G data rates above 6 GHz," *IEEE 82nd Vehicular Technology Conference (VTC2015-Fall),* 2015 Sep 6 (pp. 1-5).

[27] S. Shikhantsov, A. Thielens, G. Vermeeren, E. Tanghe, P. Demeester, L. Martens, G. Torfs, W. Joseph, "Hybrid ray-tracing/FDTD method

for human exposure evaluation of a massive MIMO technology in an industrial indoor environment," *IEEE Access*, 2019 Feb 6;7:21020-31.

[28] S. Shikhantsov, A. Thielens, G. Vermeeren, P. Demeester, L. Martens, G. Torfs, W. Joseph, "Statistical approach for human electromagnetic exposure assessment in future wireless atto-cell networks," *Radiation protection dosimetry,* 2019 May 1;183(3):326-31.

[29] International Commission on Non-Ionizing Radiation Protection. Guidelines for limiting exposure to Electromagnetic Fields (100 kHz to 300 GHz), *Health Physics*, 2020 May 1;118(5):483-524.

[30] M. Bonato, L. Dossi, E. Chiaramello, S. Fiocchi, S. Gallucci, G. Tognola, P. Ravazzani, M. Parazzini, "Single User EMF Exposure Assessment in a Case of Incoming 5G Indoor Scenario" Proceeding of International Symposium on Electromagnetic Compatibility, Virtual Conference, Italy, September 23-25

[31] The 3rd Generation Partnership Project: 3GPP TR 38.802 V14.2.0 (2017-09): "Technical Specification Group Radio Access Network; Study on New Radio Access Technology Physical Layer Aspects (Release 14)", 2017.

[32] M.-C. Gosselin, E. Neufeld, H. Moser et al., "Development of a new generation of high-resolution anatomical models for medical device evaluation: The Virtual Population 3.0," *Physics in Medicine and Biology*, 2014, vol. 59, no. 18, pp. 5287–5303.

[33] C. Gabriel, S. Gabriel and Y.E. Corthout, "The dielectric properties of biological tissues: I. Literature survey," *Physics in Medicine &Biology*, 1996, 41(11), 2231.

[34] S. Gabriel, RW. Lau, and C. Gabriel, "The dielectric properties of biological tissues: II. Measurements in the frequency range 10 Hz to 20 GHz," *Physics in Medicine &Biology*, 1996, vol. 41, pp. 2251-2269.

[35] T. Uusitupa, I. Laakso, S. Ilvonen, K. Nikoskinen, "SAR variation study from 300 to 5000 MHz for 15 voxel models including different postures," *Physics in Medicine & Biology*, 2010 Jan 28;55(4):1157.

[36] E. Chiaramello, S. Fiocchi, M. Parazzini, P. Ravazzani, J. Wiart, "Stochastic Dosimetry for Radio-Frequency Exposure Assessment in Realistic Scenarios," *Uncertainty Modeling for Engineering Applications,* 2019 (pp. 89-102). Springer, Cham.

[37] E. Chiaramello, D. Plets, S. Fiocchi, M. Bonato, G. Tognola, M. Parazzini, L. Le Brusquet, L. Martens, W. Joseph, P. Ravazzani. "Innovative Stochastic Modeling of Residential Exposure to Radio Frequency Electromagnetic Field Sources," *IEEE Journal of Electromagnetics, RF and Microwaves in Medicine and Biology*, 2020 May 14.

[38] G. Tognola, M. Bonato, E. Chiaramello, S. Fiocchi, I. Magne, M. Souques, M. Parazzini, and P. Ravazzani, "Use of Machine Learning in the analysis of indoor ELF MF exposure in children," *Int J Environ Res Public Health*, 2019, vol. 16, p. 1230-1243.

**Marta Bonato** received the master's degree in biomedical engineering from the Polytechnic of Milan, Milan, Italy, in July 2017, where she is currently working toward the Ph.D. degree in bioengineering. From September 2017 to April 2018, she was with the Institute of Electronics, Computer and Telecommunication Engineering, Consiglio Nazionale delle Ricerche, as Research Fellow. Her research interests are related to the study of the interaction of electromagnetic fields (EMF) with biological systems and the study of possible effects of EMF on health with both deterministic and stochastic dosimetry.

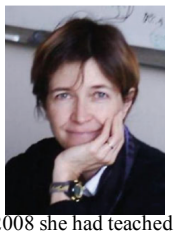

**Laura Dossi** received the degree in Electronic Engineering in 1985 from Politecnico di Milano (Italy). Since 1988 she has been a researcher at the Consiglio Nazionale delle Ricerche (CNR), initially at the Cen- tro di Studio sulle Telecomunicazioni Spaziali, which in 2002 was merged with other CNR research centres into the Istituto di Elettronica e Ingegneria Informatica e delle Telecomunicazioni (IEIIT) c/o Politecnico di Milano. From 1998 till 2008 she had teached as a lecturer at the Politecnico di Milano. Her research interests concern radio channel modelling and wireless communications.

**Emma Chiaramello** received the master's and Ph.D. degrees in biomedical engineering from the Politecnico di Torino, Torino, Italy, in 2009 and 2013, respectively. She is a Research Scientist with the Institute of Electronics, Computer and Telecommunication Engineering, National Research Council of Italy. Her scientific interests include the study of the interactions between EMF and biological systems, with both deterministic dosimetry based on computational electromagnetism methods and stochastic dosimetry based on surrogate modeling.

**Serena Fiocchi** received the master's degree in biomedical engineering in 2009 and the Ph.D. degree in bioengineering in 2014, both from the Polytechnic of Milan, Milan, Italy. She is a Research Scientist with the Institute of Electronics, Computer and Telecommunication Engineering, National Research Council of Italy. Her scientific interests include the study of the computational modeling of noninvasive brain and spinal stimulation techniques, the design and the optimization of biomedical technologies based on electromagnetic fields (EMF) for diagnostic and therapeutic applications, and the computational modeling of the interactions between EMF and biological systems.

**Silvia Gallucci** received the master's degree in biomedical engineering in 2019 from the University of Pisa (Italy). She enrolled the PhD in Bioengineering at the Politecnico di Milano for studying the EMF-human interactions. From December 2019 to April 2020 she was a research fellow at the Consiglio Nazionale delle Ricerche, Institute of Electronics, Computer and Telecommunication Engineering. Her main research interests include exposure assessment of electromagnetic fields with numerical dosimetry particularly from 5G mobile communications.

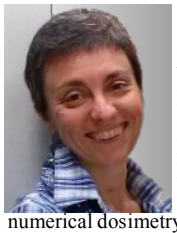

**Gabriella Tognola** received the master's degree in electronic engineering and the Ph.D. degree in bioengineering, both from Politecnico di Milano, Milan, Italy. She is currently Senior Research Scientist with the Consiglio Nazionale delle Ricerche, Institute of Electronics, Computer and Telecommunication Engineering. Her main research interests include exposure assessment of electromagnetic fields with numerical dosimetry and with Machine Learning methods and modelling of electromagnetic fields for biomedical applications.

**Paolo Ravazzani**(M'14) received the master's degree in electronic engineering and the Ph.D. degree in bioengineering, both from Politecnico di Milano, Milan, Italy. He is currently the Director of research with the Consiglio Nazionale delle Ricerche, Institute of Electronics, Computer and Telecommunication Engineering. His main research interests include exposure assessment of electromagnetic fields related to the study of the possible effects of electromagnetic fields on health and biomedical applications of electromagnetic fields.

**Marta Parazzini** (M'04) is a Research Scientist with the Institute of Electronics, Computer, and Telecommunication Engineering, Italian National Research Council, Milan, Italy. Her primary research interests include the study of the interactions of EMF with biological systems, deterministic and stochastic computational dosimetry and medical applications of EMF, in particular the techniques for noninvasive brain stimulation.